Resilience to decoherence of the macroscopic quantum superpositions generated by universally covariant optimal quantum cloning

Nicolò Spagnolo,[1,2] Fabio Sciarrino,[1,3] and Francesco De Martini[1,4,*]

[1]*Dipartimento di Fisica, Sapienza Università di Roma, piazzale Aldo Moro 5, I-00185 Roma, Italy*

[2]*Consorzio Interuniversitario per le Scienze Fisiche della Materia, piazzale Aldo Moro 5, I-00185 Roma, Italy*

[3]*Istituto Nazionale di Ottica, largo Fermi 6, I-50125 Firenze, Italy*

[4]*Accademia Nazionale dei Lincei, via della Lungara 10, I-00165 Roma, Italy*

(Received 26 February 2010; published 27 September 2010)

We show that the quantum states generated by universal optimal quantum cloning of a single photon represent a universal set of quantum superpositions resilient to decoherence. We adopt the Bures distance as a tool to investigate the persistence of quantum coherence of these quantum states. According to this analysis, the process of universal cloning realizes a class of quantum superpositions that exhibits a covariance property in lossy configuration over the complete set of polarization states in the Bloch sphere.

DOI: 10.1103/PhysRevA.82.032325 PACS number(s): 03.67.−a, 03.65.Yz, 03.65.Ta

I. INTRODUCTION

The observation of quantum properties in "macroscopic" systems has been at the focus of a long-lasting endavor to investigate the transition from the world of microscopic single-particle systems to the macroscopic "classical" domain. Uncontrolled interaction with the environment [1], that is, *decoherence*, is responsible for the progressive cancellation of the quantum properties and largely limits their experimental observation. To overcome this problem, several classes of quantum states possessing peculiar features, such as entanglement or negative Wigner distributions, have been investigated. Among them, the quantum superposition of "coherent" Glauber α states [2] and the Greenberger-Horne-Zeilinger (GHZ) states [3] have been found to be extremely fragile under decoherence, since the loss of only one particle is responsible for the cancellation of the quantum coherence present in the system.

About 10 years ago it was proposed to exploit the process of quantum cloning to generate a different class of multiphoton states (Fig. 1) [4,5]. This method recently led to the successful experimental realization of the macroscopic quantum superposition (MQS) of a large number of particles, $N \approx 5 \times 10^4$ [6,7]. The entanglement test reported in Ref. [7] for the collinear amplification regime was recently discussed by Sekatski *et al.* [8] Later, a recent paper [9] reported a detailed theoretical analysis of the adopted entanglement criteria and showed that a substantial degree of entanglement was indeed present in the micro-macro system dealt with in [7].

The persistence of quantum coherence in MQS states realized by phase-covariant cloning, that is, limited to a *one-dimensional* subspace of the entire Bloch sphere of the macroqubit, was analyzed on the basis of two criteria based on the definition of "distance" in the Hilbert space [10,11]. It was found that this limited physical system shows a high resilience to decoherence at variance with coherent $|\alpha\rangle$ state MQS. The feature of phase-covariance symmetry mostly consists of the relative simplicity of the required "collinear" structure and of the high efficiency of quantum-injected optical parametric amplification (QI-OPA). This one amplifies equally well the single-photon polarization states $|\phi\rangle$ belonging to the equatorial plane of the Bloch sphere of the injected microqubit [5,6].

Given this circumstance, the question arose whether there exists a physical system that exhibits the property of resilience to decoherence in a larger Hilbert space or, better, in the full space available to the generated macrostate. The present paper addresses this question. The "universal quantum cloning machine" realized in its "optimal" MQS mode nondegenerate configuration possesses the required property: resilience to decoherence is realized in the full Hilbert space spanned by the output macrostate [4,12–14].

In this paper, we report a theoretical analysis of the resilience to decoherence of quantum states generated by universal quantum cloning of a single-photon qubit. The basic tools of this investigation are provided by the two coherence criteria defined in Refs. [10] and [11]. There, the Bures distance [15–17]

$$\mathcal{D}(\hat{\rho},\hat{\sigma}) = \sqrt{1-\sqrt{\mathcal{F}(\hat{\rho},\hat{\sigma})}}, \tag{1}$$

where $\mathcal{F}$ is a quantum "fidelity," has been adopted as a measure to quantify (I) the "distinguishability" between two quantum states $\{|\phi_1\rangle,|\phi_2\rangle\}$ and (II) the *degree of coherence*, that is, the MQS visibility, of their quantum superpositions $|\phi^{\pm}\rangle = 2^{-1/2}(|\phi_1\rangle \pm |\phi_2\rangle)$. These criteria were chosen according to the following considerations. (I) The distinguishability, that is, the degree of orthogonality, represents the maximum discrimination power among two quantum states available within a measurement. (II) The related visibility between the superposition $|\phi^+\rangle$ and the superposition $|\phi^-\rangle$ depends exclusively on the relative phase of the component states $|\phi_1\rangle$ and $|\phi_2\rangle$. Consider two orthogonal superpositions $|\phi^{\pm}\rangle$: $\mathcal{D}(|\phi^+\rangle,|\phi^-\rangle) = 1$. In the presence of decoherence the relative phase between $|\phi_1\rangle$ and $|\phi_2\rangle$ progressively randomizes and the superpositions $|\phi^+\rangle$ and $|\phi^-\rangle$ approach an identical fully mixed state leading to $\mathcal{D}(|\phi^+\rangle,|\phi^-\rangle) = 0$. The physical interpretation of $\mathcal{D}(|\phi^+\rangle,|\phi^-\rangle)$ as the visibility of a superposition $|\phi^{\pm}\rangle$ is legitimate insofar as the component states of the corresponding superpositions, $|\phi_1\rangle$ and $|\phi_2\rangle$ may be defined, at least approximately, as *pointer states* or *einselected states* [1]. Within the set of eigenstates characterizing any quantum

*francesco.demartini@uniroma1.it

 ©2010 The American Physical Society

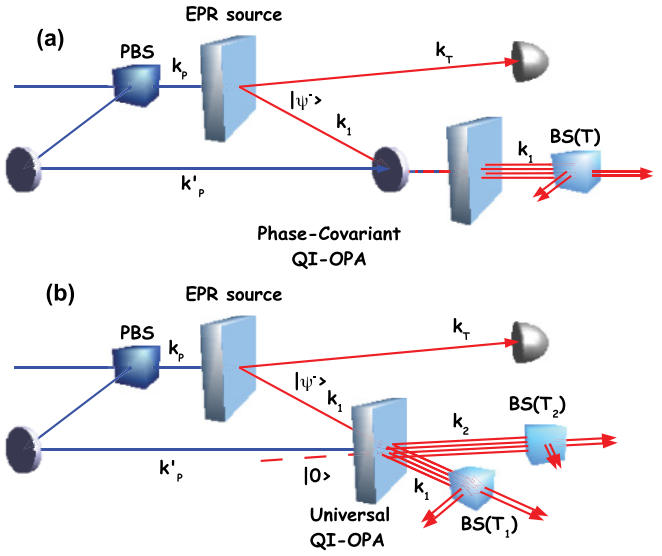

FIG. 1. (Color online) (a) Scheme for the phase-covariant cloning of a single-photon state with a collinear optical parametric amplifier. The beam splitter [BS(T)] is inserted to simulate propagation over lossy channels of the output field. (b) Scheme for the universal cloning of a single-photon state with a noncollinear optical parametric amplifier: BSs on spatial modes $\mathbf{k}_1$ [BS(T_1)] and $\mathbf{k}_2$ [BS(T_2)].

system, pointer states are defined as those least affected by external noise and that are highly resilient to decoherence. In other words, pointer states are "quasiclassical" states which realize the minimum flow of information from (or to) the system to (or from) the environment. They are involved in all criteria of classicality, such as those based on the "purity" and "predictability" of the macrostates [1].

Our interest is focused on the resilience properties of different classes of quantum states after propagation over a lossy channel. This is modeled by a linear beam splitter (BS) with transmittivity T and reflectivity $R = 1 - T$ acting on a state $\widehat{\rho}$ associated with a single BS input mode (Fig. 1). Let us first analyze the behavior of the coherent states and their superpositions. Investigation of the Glauber's states leading to the α-MQS case [2], $|\Phi_{\alpha\pm}\rangle = \mathcal{N}^{-1/2}(|\alpha\rangle \pm |-\alpha\rangle)$, in terms of the pointer states' $|\pm\alpha\rangle$ leads to the closed-form result $\mathcal{D}(|\Phi_{\alpha+}\rangle,|\Phi_{\alpha-}\rangle) = \sqrt{1-\sqrt{1-e^{-4R|\alpha|^2}}}$. This is plotted in Fig. 2 (dashed line) as a function of the average number of lost photons: $x \equiv R\langle n\rangle$. Note that the value of $\mathcal{D}(|\Phi_{\alpha+}\rangle,|\Phi_{\alpha-}\rangle)$ drops from 1 to 0.095 upon loss of just one photon: $x = 1$. In other words, the superpositions of α states $|\Phi_{\alpha\pm}\rangle = \mathcal{N}^{-1/2}(|\alpha\rangle \pm |-\alpha\rangle)$ exhibit a fast decrease in their coherence, that is, their visibility and distinguishability, while the related components $|\pm\alpha\rangle$, that is, the pointer states [1], remain distinguishable until all photons in the state are depleted by the BS.

The amplification QI-OPA systems under investigation are reported in Fig. 1. An Einstein-Podolsky-Rosen (EPR) pair $|\psi^-\rangle = 2^{-1/2}(|H\rangle_1|V\rangle_T - |V\rangle_1|H\rangle_T)$ is generated in a first nonlinear crystal. H and V refer to horizontal and vertical field polarizations, that is, the extreme poles of the Poincaré sphere. By analyzing and measuring the polarization of the photon associated with mode $\mathbf{k}_T$, the photon on mode $\mathbf{k}_1$ is nonlocally prepared in the polarization qubit: $|\psi\rangle_1 = \cos(\theta/2)|H\rangle_1 + e^{i\phi}\sin(\theta/2)|V\rangle_1$. Then by accurate spatial focusing, the single photon in state $|\psi\rangle_1$ is injected into the amplifier simultaneously with the strong UV pump beam $\mathbf{k}'_P$. Let us analyze the two configurations of the apparatus leading, as said, to two different regimes of quantum cloning: phase covariant and universal.

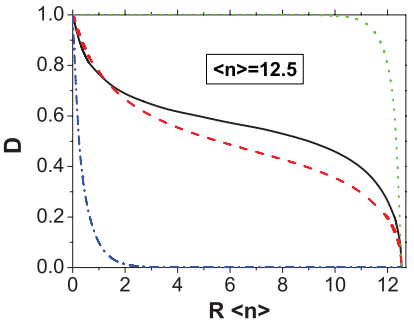

FIG. 2. (Color online) Bures distance for various classes of MQSs for $\langle n\rangle = 12.5$. The lower (blue) dash-dotted curve corresponds to the quantum superpositions of coherent states $|\alpha\rangle \pm |-\alpha\rangle$, while the dotted (green) upper curve is relative to the distinguishability between component states $|\pm\alpha\rangle$. The solid (black) curve corresponds to the MQS generated by phase-covariant cloning [10,11], while the dashed (red) curve corresponds to the universal-cloning-based MQS.

II. PHASE-COVARIANT OPTIMAL QUANTUM CLONING MACHINE

Let us first briefly review the results obtained for a "collinear" optical configuration, that is, leading to a phase-covariant optimal quantum cloning machine [Fig. 1(a)] [7]. The interaction Hamiltonian of this process is $\widehat{\mathcal{H}}_{\rm PC} = i\hbar\chi\widehat{a}_H^\dagger\widehat{a}_V^\dagger + \text{H.c.}$ in the $\{\vec{\pi}_H,\vec{\pi}_V\}$ polarization basis, and $\widehat{\mathcal{H}}_{\rm PC} = \frac{i\hbar\chi}{2}e^{-i\phi}(\widehat{a}_\phi^{\dagger 2} - \widehat{a}_{\phi_\perp}^{\dagger 2}) + \text{H.c.}$ for any "equatorial" basis $\{\vec{\pi}_\phi,\vec{\pi}_{\phi\perp}\}$ on the Poincaré sphere having as poles the states $\vec{\pi}_H$ and $\vec{\pi}_V$. The relevant equatorial bases considered here are $\{\vec{\pi}_+,\vec{\pi}_-\}$ and $\{\vec{\pi}_R,\vec{\pi}_L\}$, corresponding, respectively, to $\phi = 0$ and $\phi = \pi/2$. The amplified state for an injected equatorial qubit is

$$\left|\Phi_{\rm PC}^{\phi}\right\rangle = \sum_{i,j=0}^{\infty}\gamma_{ij}|(2i+1)\phi,(2j)\phi_\perp\rangle, \tag{2}$$

where $\gamma_{ij} = \frac{1}{C^2}(e^{-i\phi}\frac{\Gamma}{2})^i(-e^{i\phi}\frac{\Gamma}{2})^j\frac{\sqrt{(2i+1)!}\sqrt{(2j)!}}{i!j!}$, $C = \cosh g$, $\Gamma = \tanh g$. Hereafter, $|p\psi,q\psi_\perp\rangle_i$ stands for a Fock state with p photons polarized $\vec{\pi}_\psi$ and q photons polarized $\vec{\pi}_{\psi_\perp}$ on spatial mode $\mathbf{k}_i$. We evaluated numerically the distinguishability of $\{|\Phi_{\rm PC}^{+,-}\rangle\}$ through the distance $\mathcal{D}(|\Phi_{\rm PC}^{+}\rangle,|\Phi_{\rm PC}^{-}\rangle)$ (Fig. 2). Consider the MQS of the macrostates $|\Phi_{\rm PC}^{+}\rangle$, $|\Phi_{\rm PC}^{-}\rangle$: $|\Psi_{\rm PC}^{\pm}\rangle = \frac{\mathcal{N}_\pm}{\sqrt{2}}(|\Phi_{\rm PC}^{+}\rangle \pm i|\Phi_{\rm PC}^{-}\rangle)$. Due to the linearity of the amplification process [12], $|\Psi_{\rm PC}^{\pm}\rangle = |\Phi_{\rm PC}^{R/L}\rangle$ and in virtue of the phase covariance of the process,

$$\mathcal{D}(|\Psi_{\rm PC}^{+}\rangle,|\Psi_{\rm PC}^{-}\rangle) = \mathcal{D}\left(\left|\Phi_{\rm PC}^{R}\right\rangle,\left|\Phi_{\rm PC}^{L}\right\rangle\right) = \mathcal{D}(|\Phi_{\rm PC}^{+}\rangle,|\Phi_{\rm PC}^{-}\rangle). \tag{3}$$

These equations can be assumed as the theoretical conditions assuring the resilience to decoherence of any quantum MQS

(q-MQS) state generated by the QI-OPA in the collinear configuration: they identify the equatorial set of the Bloch sphere as a privileged resilience-to-decoherence Hilbert subspace. The visibility of the q-MQS $\{|\Psi_{\mathrm{PC}}^{+,-}\rangle\}$ was evaluated numerically analyzing the Bures distance as a function of x. Note that for small values of x the decay of $D(x)$ is far slower than for the coherent α-MQS case. This resilience-to-decoherence feature has been experimentally verified in [7].

III. UNIVERSAL OPTIMAL QUANTUM CLONING MACHINE

Let us now investigate the resilience to decoherence of the MQS generated by the *universal optimal quantum cloning machine*. According to the original proposal, this was implemented experimentally by a QI-OPA device working in a noncollinear, that is, mode nondegenerate, configuration [Fig. 1(b)] [4]. This parametric amplifier acts as a universal $N \to M$ quantum cloning machine [18,19] as well as a universal-NOT (UNOT) quantum machine [20]. The interaction Hamiltonian for the amplifier is now given by $\hat{\mathcal{H}}_U = i\hbar\chi(\hat{a}^\dagger_{1\psi}\hat{a}^\dagger_{2\psi_\perp} - \hat{a}^\dagger_{1\psi_\perp}\hat{a}^\dagger_{2\psi}) + \mathrm{H.c.}$, where $\vec{\pi}_\psi = \cos(\theta/2)\vec{\pi}_H + e^{i\phi}\sin(\theta/2)\vec{\pi}_V$ and $\vec{\pi}_{\psi_\perp} = (\vec{\pi}_\psi)^\perp$. Since this system possesses a complete SU(2) simmetry, the Hamiltonian maintains the same form for any simultaneous rotation of the Bloch sphere of the polarization basis for both output modes, $\mathbf{k}_1$ and $\mathbf{k}_2$.

The output state of the amplifier reads

$$|\Phi_U^{1\psi}\rangle = \hat{U}|1\psi\rangle_1 = \frac{1}{C^3}\sum_{n,m=0}^{\infty}\Gamma^{n+m}(-1)^m\sqrt{n+1} \times |(n+1)\psi, m\psi_\perp\rangle_1 \otimes |m\psi, n\psi_\perp\rangle_2. \quad (4)$$

We note that the multiphoton quantum superposition state $|\Phi_U^{1\psi}\rangle = \cos(\theta/2)|\Phi_U^{1H}\rangle + e^{i\phi}\sin(\theta/2)|\Phi_U^{1V}\rangle$ and $|\Phi_U^{1\psi_\perp}\rangle$ lives in the joint system composed by the $\mathbf{k}_1$ and $\mathbf{k}_2$ spatial modes. More specifically, the photons generated on mode $\mathbf{k}_1$, to which we refer as the *cloning* mode, present the property of being as close as possible, according to the laws of quantum mechanics, to the injected single-photon state. On the contrary, photons generated on mode $\mathbf{k}_2$, to which we refer as the *anticloning* mode, present a polarization state as close as possible to $|\psi_\perp\rangle$ [20]. Hence, both spatial modes carry out information on the single photon injected into the amplifier. To investigate the features of the state of Eq. (4), Fig. 3 reports the photon-number distribution for the reduced states $\hat{\rho}_{U\mathbf{k}_i}^{1\psi(1\psi_\perp)} = \mathrm{Tr}_{\mathbf{k}_i}(|\Phi_U^{1\psi(1\psi_\perp)}\rangle\langle\Phi_U^{1\psi(1\psi_\perp)}|)$ associated with the output spatial modes $\mathbf{k}_1$ and $\mathbf{k}_2$. The photon-number distributions in the $\mathbf{k}_1$ spatial mode [Figs. 3(a) and 3(c)], that is, the cloning mode, show strong imbalance along the direction of the injected polarization state. The anticloning $\mathbf{k}_2$ mode [Figs. 3(b) and 3(d)] presents the opposite imbalance along the direction of the orthogonal polarization, since in that spatial mode the amplifier works as a UNOT machine [20]. This feature is also illuminated by the contour plots in Figs. 3(e) through 3(h), where the white regions represent the Fock-space zones where the photon-number distributions are more densely populated. Furthermore, we note that, at variance with the phase-covariant amplifier [10,11], the output states do not exhibit any comb structure in their photon-number distributions. In agreement with the universality property of the source, the Bures distance between the MQS states $|\Phi_U^{1\psi}\rangle = \cos(\theta/2)|\Phi_U^{1H}\rangle + e^{i\phi}\sin(\theta/2)|\Phi_U^{1V}\rangle$ and $|\Phi_U^{1\psi_\perp}\rangle$ is independent of the choice of (θ,ϕ):

$$\mathcal{D}(\hat{\rho}_U^{1\psi}, \hat{\rho}_U^{1\psi_\perp}) = \mathcal{D}(\hat{\rho}_U^{1\psi'}, \hat{\rho}_U^{1\psi'_\perp}) \quad (5)$$

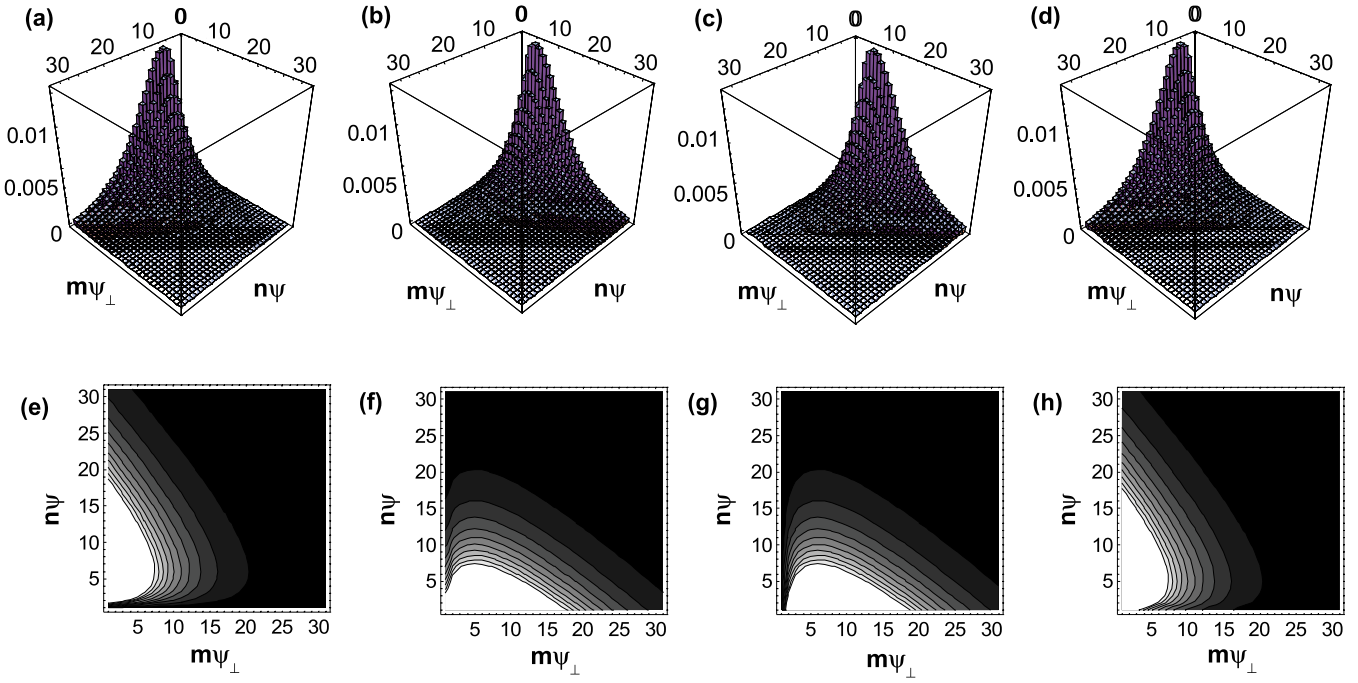

FIG. 3. (Color online) Probability distribution (a)–(d) and contour plots (e)–(h) of the reduced density matrices $\hat{\rho}_{\mathbf{k}_1}^{1\psi}$ (a),(e), $\hat{\rho}_{\mathbf{k}_2}^{1\psi}$ (b),(f), $\hat{\rho}_{\mathbf{k}_1}^{1\psi_\perp}$ (c),(g), and $\hat{\rho}_{\mathbf{k}_2}^{1\psi_\perp}$ (d),(h). All plots correspond to the gain value $g = 1.5$.

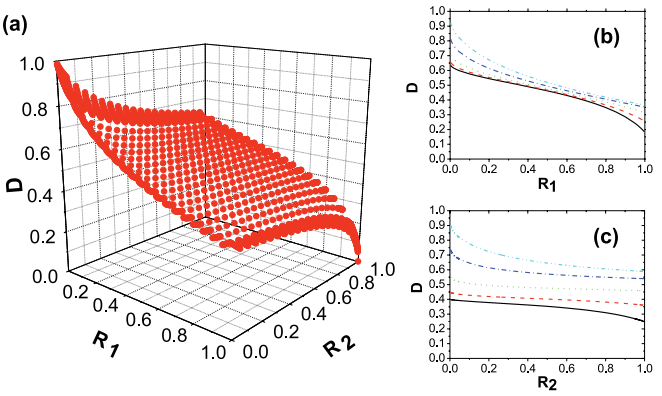

FIG. 4. (Color online) Bures distance between the MQSs $|\Phi^{1\psi}\rangle$ and $|\Phi^{1\psi_\perp}\rangle$ after losses. (a) Three-dimensional surface $\mathcal{D}(R_1,R_2)$ as a function of the two spatial mode parameters $R_1 = 1 - T_1$ and $R_2 = 1 - T_2$. (b) $\mathcal{D}(R_1,R_2)$, with R_2 fixed, as a function of R_1. (c) $\mathcal{D}(R_1,R_2)$, with R_1 fixed, as a function of R_2. (b, c) Solid curves correspond to $R_{2(1)} = 0.9$; dashed curves, to $R_{2(1)} = 0.75$; dotted curves, to $R_{2(1)} = 0.5$; dash-dotted curves, to $R_{2(1)} = 0.2$; and dash-dot-dotted curves, to $R_{2(1)} = 0.05$.

for any basis $\{\vec{\pi}_\psi,\vec{\pi}_{\psi'}\}$. This feature is the extension of the ϕ-covariance property of the collinear quantum cloning machine [11] to the full set of polarization states on the output Bloch sphere. As stated, the Bures distance must be evaluated considering the joint cloning-anticloning multiphoton state.

By introducing, in analogy with the previous case, two BSs (BS_1 and BS_2) in the output states, we evaluate by standard algebraic numerical routines the Bures distance between the orthogonal macrostates $|\Phi_U^{1\psi}\rangle$ and $|\Phi_U^{1\psi_\perp}\rangle$ as a function of the corresponding transmission parameters T_1 and T_2. In Fig. 4(a) we report a three-dimensional plot of the function $\mathcal{D}(R_1,R_2) = \mathcal{D}(\hat{\rho}^{1\psi},\hat{\rho}^{1\psi_\perp})$ for a gain value of $g = 1.2$, corresponding to an overall average number of photons $\langle\hat{n}\rangle = \sum_{i=1}^{2}[\langle\hat{n}_{i\psi}\rangle + \langle\hat{n}_{i\psi_\perp}\rangle] \approx 15$. Figure 4(a) shows that the MQS visibility possesses a resilient structure in the presence of losses, since the Bures distance does not decrease exponentially with the lossy parameters $\{R_1,R_2\}$. In Figs. 4(b) and 4(c) we report several sections of the three-dimensional surface in Fig. 4(a) by fixing either R_1 or R_2. We note that the $|\Phi_U^{1\psi}\rangle$ and $|\Phi_U^{1\psi_\perp}\rangle$ MQSs are more sensitive to losses in the cloning mode $\mathbf{k}_1$ than in the anticloning mode $\mathbf{k}_2$. This can be explained by considering that the distance between these orthogonal macrostates depends on the imbalance in the corresponding photon-number distributions. Since this feature is pronounced in the spatial cloning mode $\mathbf{k}_1$, losses acting on this mode cancel more rapidly the orthogonality between $|\Phi_U^{1\psi}\rangle$ and $|\Phi_U^{1\psi_\perp}\rangle$. As the number of photons present in the state is increased, the visibility stays large up to a value $V \approx 0.5$ over a larger range of the number of reflected photons. All this shows that, in analogy with the phase-covariant case, the MQSs generated by quantum cloning become more resilient to losses since the quantum coherence present in these states can survive the loss of a larger number of photons.

Finally, we analyze the action of the orthogonality filter on the amplified single-photon states $|\Phi_U^{1\psi}\rangle$ by analyzing how the Bures distance is affected by the application of this device. The positive operator-valued measurement (POVM)-like

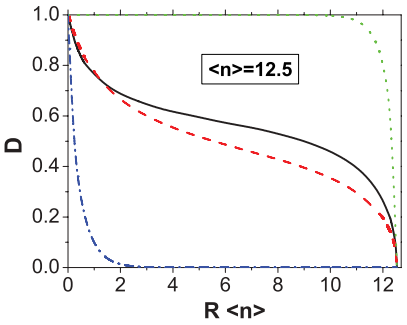

FIG. 5. (Color online) Numerical results for the Bures distance between the $|\Phi^{1\psi}\rangle$ and $|\Phi^{1\psi_\perp}\rangle$ states after propagation over a lossy channel and application of the orthogonality filter device. From the lower to the upper curve, the filtering threshold is set to $k = 0\langle n\rangle$ ($P_{\rm filt} = 1$), $k = 2\langle n\rangle$ ($P_{\rm filt} = 1.7 \times 10^{-1}$), $k = 4\langle n\rangle$ ($P_{\rm filt} = 1.5 \times 10^{-2}$), $k = 6\langle n\rangle$ ($P_{\rm filt} = 1.1 \times 10^{-3}$), and $k = 8\langle n\rangle$ ($P_{\rm filt} = 8.2 \times 10^{-5}$). All curves are calculated for a gain $g = 1.2$, corresponding to an average number of generated photons on mode $\mathbf{k}_1$ equal to $\langle n\rangle \simeq 8$.

technique [21] implied by this device locally selects the events for which the difference between the photon numbers associated with two orthogonal polarizations $|m - n| > k$, that is, larger than an adjustable threshold k [6]. By this method a sharper discrimination between the output states $|\Phi_U^{1\psi}\rangle$ and $|\Phi_U^{1\psi_\perp}\rangle$ can be achieved. We focus our attention only on the reduced density matrix $\hat{\rho}_{\mathbf{k}_1}^{1\psi}(T)$ corresponding to the output spatial mode $\mathbf{k}_1$. We then apply the numerical methods previously adopted in order to calculate the Bures distance $\mathcal{D}(x)$, where $x = R\langle n\rangle$ is the number of lost photons, as a function of the threshold k. In Fig. 5 the results of a numerical analysis carried out for $g = 1.2$ and different values of k are reported.

Note the increase in the value of $\mathcal{D}(x)$, that is, of the MQS Visibility, by increasing k. Of course, in the spirit of any POVM, the high interference visibility is achieved here at the cost of a lower success probability [22]. The general, most important feature shown by all these figures is that both the distinguishability and the visibility of all universal macrostates $|\Phi_U^{1\psi}\rangle, |\Phi_U^{1\psi_\perp}\rangle$, as well as of all their universal quantum superpositions, can be kept close to a high value despite the increasing effect of decoherence due to increasing values of the BS_1 reflectivity: $R\langle n\rangle$. On the basis of all these results we may then conclude that all the universal macrostates and superpositions generated by the QI-OPA may be safely defined as classically stable, einselected pointer states [1].

IV. CONCLUSIONS

The present paper reports a thorough theoretical analysis of the resilience to decoherence of the quantum superpositions generated by universal quantum cloning. This property is found to depend on the symmetry ("covariance") of the optimal cloning process, which allows identification of a covariant set of stable quantum superpositions over the full Hilbert space spanned by the generated macrostates. To gain insight into the general picture and to support the congruence of our final conclusions, we find it useful to relate here the various aspects

of the optimal cloning process with the current MQS physical model considered in [1].

(1) The system in our optical entangled amplification scheme is represented by the assembly of $N+1$ photon particles associated with the macrostate $|\Phi^{\phi}\rangle$ generated by the optimal cloning apparatus.

(2) The flow of (classical) "noise information" directed from the environment toward the system is attributed to the unavoidable squeezed-vacuum noise affecting the building-up of the macrostate $|\Phi^{\phi}\rangle$ within the process of amplification. As already stressed, the optimality of the quantum cloning generally implies that the flow of classical noise is the minimum allowed by the principles of quantum mechanics, that is, by the "no-cloning theorem" [23,24].

(3) The flow of quantum information directed from the system toward the environment is provided by the controlled "decoherence in action" provided by the BS-scattering process and by the losses taking place in all photodetection processes. We have seen that by the use of the orthogonality filter, or even in the absence of it, the interference phase-distrupting effects caused by the decoherence can be efficiently tamed for macrostates and for their quantum superpositions.

(4) By the universal cloning method considered here the maximum allowed distinguishability and visibility are attained for the macroqubit Hilbert space.

(5) In any cloning apparatus a unitary transformation $\hat{U}$ connects all physical properties belonging to the microworld to the corresponding ones belonging to the macrosopic "classical" world. Any lack of perceiving this close correspondence must be attributable only to the intrinsic limitations of our perceiving senses, of our observational methods, or of our measurement apparatuses. In other words, at least in our case, the two worlds are deterministically mirrored one into the other by the unitary map $\hat{U}$, which is provided by quantum mechanics itself. This is the key to understanding our results.

(6) The q-MQS based on the cloning process is not a "thermodynamic" system, as its dynamics and decoherence do not depend on the temperature T. Rather, it belongs to the class of the "parametrically driven, open quantum-statistical systems" that have recently been invoked to provide and sustain extended long-range nonlocal coherence processes in complex biological photosyntetic systems [25,26].

ACKNOWLEDGMENTS

We acknowledge support by the "Futuro in Ricerca" Project HYTEQ, and Progetto d'Ateneo of Sapienza Università di Roma.

APPENDIX: CALCULATION OF THE DENSITY MATRIX COEFFICIENTS FOR THE UNIVERSALLY AMPLIFIED SINGLE-PHOTON STATES IN THE PRESENCE OF LOSSES

In this appendix we report the detailed calculation of the coefficient of the density matrix for the $|\Phi^{1\psi}\rangle$ states in the presence of losses. We focus our attention on the $|1\psi\rangle_1$ case only, since the calculation for the complementary state $|1\psi_\perp\rangle_1$ is similar.

First, we investigate the features of the interaction Hamiltonian. Due to the properties of $\hat{\mathcal{H}}_U$, the time evolution operator in the interaction picture $\hat{U}=\exp(-i\hat{\mathcal{H}}_U t/\hbar)$ can be decomposed as the product of two independent operators $\hat{U}=\hat{U}_{\mathcal{A}}\otimes\hat{U}_{\mathcal{A}'}$, acting on two different Hilbert spaces corresponding to the two sets of modes $\mathcal{A}\equiv\{(\mathbf{k}_1,\vec{\pi}_\psi),(\mathbf{k}_2,\vec{\pi}_{\psi_\perp})\}$ and $\mathcal{A}'\equiv\{(\mathbf{k}_1,\vec{\pi}_{\psi_\perp}),(\mathbf{k}_2,\vec{\pi}_\psi)\}$ [18,19]:

$$\hat{U}_{\mathcal{A}}=\exp[\chi t(\hat{a}^\dagger_{1\psi}\hat{a}^\dagger_{2\psi_\perp}-\hat{a}_{1\psi}\hat{a}_{2\psi_\perp})], \tag{A1}$$

$$\hat{U}_{\mathcal{A}'}=\exp[-\chi t(\hat{a}^\dagger_{1\psi_\perp}\hat{a}^\dagger_{2\psi}-\hat{a}_{1\psi_\perp}\hat{a}_{2\psi})]. \tag{A2}$$

In the case of a separable input state in the QI-OPA $\hat{\rho}=\hat{\rho}_{\mathcal{A}}\otimes\hat{\rho}_{\mathcal{A}'}$, the amplified states can be written in a separable form:

$$\hat{\rho}(t)=\hat{U}\hat{\rho}\hat{U}^\dagger=(\hat{U}_{\mathcal{A}}\hat{\rho}_{\mathcal{A}}\hat{U}^\dagger_{\mathcal{A}})\otimes(\hat{U}_{\mathcal{A}'}\hat{\rho}_{\mathcal{A}'}\hat{U}^\dagger_{\mathcal{A}'}). \tag{A3}$$

This separability property is exploited in the remainder of this paper both for calculation of the density matrix after losses and for evaluation of the Bures distance.

1. Density matrix coefficients for amplified states

In this section we derive the density matrix coefficients for the amplified states $|\Phi^{1\psi(1\psi_\perp)}\rangle$ after transmission over a lossy channel. We focus our attention on the $|1\psi\rangle_1$ case only, since the calculation of the complementary state $|1\psi_\perp\rangle_1$ is similar. Due to the property of the universal amplifier analyzed previously, we analyze separately the two subspaces $\mathcal{A}$ and $\mathcal{A}'$ [Eq. (A3)]. Since the time evolution operators $\hat{U}_{\mathcal{A}}$ and $\hat{U}_{\mathcal{A}'}$ are equivalent apart from a global phase factor (-1), the quantum states for the amplifier $\mathcal{A}'$ can be directly derived from the expressions obtained for amplifier $\mathcal{A}$. Only two relevant cases are considered: the vacuum injected state $\hat{U}_{\mathcal{A}}|0\rangle$ (spontaneous emission) and the single-photon injected state $\hat{U}_{\mathcal{A}}|1\psi\rangle_1$. This analysis can be performed separately for the two amplifiers since the separability feature also holds after the amplified state propagates over a lossy channel in both $\mathbf{k}_1$ and $\mathbf{k}_2$ spatial modes. This is a consequence of the properties of the lossy channel map, which, being a "local" transformation, acts independently on each mode. The output state after losses reads

$$\mathcal{L}[\hat{\rho}(t)]=\mathcal{L}_{\mathcal{A}}[\hat{U}_{\mathcal{A}}\hat{\rho}_{\mathcal{A}}\hat{U}^\dagger_{\mathcal{A}}]\otimes\mathcal{L}_{\mathcal{A}'}[\hat{U}_{\mathcal{A}'}\hat{\rho}_{\mathcal{A}'}\hat{U}^\dagger_{\mathcal{A}'}]. \tag{A4}$$

Here $\mathcal{L}_{\mathcal{A}}=\mathcal{L}_{\mathbf{k}_1,\vec{\pi}_\psi}\otimes\mathcal{L}_{\mathbf{k}_2,\vec{\pi}_{\psi_\perp}}$, $\mathcal{L}_{\mathcal{A}'}=\mathcal{L}_{\mathbf{k}_1,\vec{\pi}_{\psi_\perp}}\otimes\mathcal{L}_{\mathbf{k}_2,\vec{\pi}_\psi}$ are the maps induced by losses for the two subspaces, where the single-mode map $(\mathbf{k}_i,\vec{\pi})$ is given by the following expression [27]:

$$\mathcal{L}_{\mathbf{k}_i,\vec{\pi}}[\hat{\sigma}]=\sum_{p=0}^{\infty}R_i^{p/2}T_i^{(\hat{a}^\dagger\hat{a})/2}\frac{\hat{a}^p_{\mathbf{k}_i,\vec{\pi}}}{\sqrt{p!}}\hat{\sigma}\frac{\hat{a}^{\dagger p}_{\mathbf{k}_i,\vec{\pi}}}{\sqrt{p!}}T_i^{(\hat{a}^\dagger\hat{a})/2}R_i^{p/2}, \tag{A5}$$

with T_i, the transmission efficiency of the channel, assumed to be polarization independent.

We begin with the analysis of the spontaneous emission regime. The calculation proceeds as follows. Starting from the quantum state for the subsystem $\mathcal{A}$ $\hat{U}_{\mathcal{A}}|0\rangle$, the output state after transmission over the lossy channel is obtained by applying the lossy channel map (A5) to the density matrix of state $\hat{\rho}^0_{\mathcal{A}}$. The same procedure applies for single-photon amplified states, where the seed of the amplifier $\mathcal{A}$ is the single-photon state $|1\psi\rangle$. In this case, the input state in the lossy channel is $\hat{U}_{\mathcal{A}}|1\psi\rangle_1$. By applying the lossy channel map over the density

matrix $\hat{\rho}_{\mathcal{A}}^{1\psi}$ of the state, we find the desired output states. Details on the calculation and the complete expressions of the coefficients for the density matrices $\hat{\rho}_{\mathcal{A}}^{1\psi}(T_1,T_2)$ and $\hat{\rho}_{\mathcal{A}}^{0}(T_1,T_2)$ are reported here.

Let us emphasize that, due to analogy of the Hamiltonians of the two amplifiers $\mathcal{A}$ and $\mathcal{A}'$, the density matrices of states $\hat{\rho}_{\mathcal{A}'}^{0}(T_1,T_2)$ and $\hat{\rho}_{\mathcal{A}'}^{1\psi_\perp}(T_1,T_2)$ for amplifier $\mathcal{A}'$ can be directly derived from Eqs. (A8)–(A10) and (A13)–(A15) by substituting (Γ) with $(-\Gamma)$ and by relabeling the indexes describing the spatial and polarization modes.

We begin with analysis of the spontaneous emission regime. The quantum state for subsystem $\mathcal{A}$ is given by

$$\hat{U}_{\mathcal{A}}|0\rangle = \frac{1}{C}\sum_{n=0}^{\infty}\Gamma^n|n\psi\rangle_1\otimes|m\psi_\perp\rangle_2. \tag{A6}$$

The output state after transmission over the lossy channel is obtained by applying the lossy channel map (A5) to the density matrix of state $\hat{\rho}_{\mathcal{A}}^{0}$:

$$\hat{\rho}_{\mathcal{A}}^{0}(T_1,T_2) = \left(\mathcal{L}_{\mathbf{k}_1,\vec{\pi}_\psi}\otimes\mathcal{L}_{\mathbf{k}_2,\vec{\pi}_{\psi_\perp}}\right)\left[\hat{\rho}_{\mathcal{A}}^{0}\right]. \tag{A7}$$

After direct application of the lossy channel map to the density matrix, the following expression is obtained:

$$\begin{aligned}\hat{\rho}_{\mathcal{A}}^{0}(T_1,T_2) = &\sum_{i=0}^{\infty}\sum_{j=0}^{i}\sum_{k=i-j}^{\infty}\left[\hat{\rho}_{\mathcal{A}}^{0}(T_1,T_2)\right]_{ijk}^{(i\geqslant j)}|i\psi\rangle_1\langle k\psi|\\ &\otimes|j\psi_\perp\rangle_2\langle(j+k-i)\psi_\perp|\\ &+\sum_{i=0}^{\infty}\sum_{j=i+1}^{\infty}\sum_{k=0}^{\infty}\left[\hat{\rho}_{\mathcal{A}}^{0}(T_1,T_2)\right]_{ijk}^{(i<j)}|i\psi\rangle_1\langle k\psi|\\ &\otimes|j\psi_\perp\rangle_2\langle(j+k-i)\psi_\perp|,\end{aligned} \tag{A8}$$

where the coefficients for $i\geqslant j$ and $i<j$ are given by

$$\begin{aligned}\left[\hat{\rho}_{\mathcal{A}}^{0}(T_1,T_2)\right]_{ijk}^{(i\geqslant j)} = &\frac{1}{C^2}\Gamma^{i+k}\frac{T_1^{(i+k)/2}T_2^{(2j+k-i)/2}R_2^{i-j}\sqrt{i!k!}}{(i-j)!\sqrt{j!(j+k-i)!}}\\ &\times{}_2F_1(1+i,1+k,i+i-j;\Gamma^2R_1R_2),\end{aligned} \tag{A9}$$

$$\begin{aligned}&\left[\hat{\rho}_{\mathcal{A}}^{0}(T_1,T_2)\right]_{ijk}^{(i<j)}\\ &=\frac{1}{C^2}\Gamma^{2j+k-i}\frac{T_1^{(i+k)/2}T_2^{(2j+k-i)/2}R_1^{j-i}\sqrt{j!(j+k-i)!}}{(j-i)!\sqrt{i!k!}}\\ &\quad\times{}_2F_1(1+j,1+j+k-i,1+j-i;\Gamma^2R_1R_2),\end{aligned} \tag{A10}$$

where ${}_2F_1(a,b,c;z)$ is the hypergeometric function defined in Ref. [28]. The same procedure has been applied to the stimulated case, where the seed of the amplifier $\mathcal{A}$ is the single-photon state $|1\psi\rangle$. In this case, the input state in the lossy channel has the following expression:

$$\hat{U}_{\mathcal{A}}|1\psi\rangle_1 = \frac{1}{C^2}\sum_{n=0}^{\infty}\Gamma^n\sqrt{n+1}|(n+1)\psi\rangle_1\otimes|m\psi_\perp\rangle_2. \tag{A11}$$

By applying the lossy channel map over the density matrix $\hat{\rho}_{\mathcal{A}}^{1\psi}$ of the state, we find

$$\hat{\rho}_{\mathcal{A}}^{1\psi}(T_1,T_2) = \left(\mathcal{L}_{\mathbf{k}_1,\vec{\pi}_\psi}\otimes\mathcal{L}_{\mathbf{k}_2,\vec{\pi}_{\psi_\perp}}\right)\left[\hat{\rho}_{\mathcal{A}}^{1\psi}\right]. \tag{A12}$$

Application of the map leads to the following expression for the density matrix:

$$\begin{aligned}\hat{\rho}_{\mathcal{A}}^{1\psi}(T_1,T_2) = &\sum_{i=0}^{\infty}\sum_{j=0}^{i-1}\sum_{k=i-j}^{\infty}\left[\hat{\rho}_{\mathcal{A}}^{1\psi}(T_1,T_2)\right]_{ijk}^{(i\geqslant j+1)}|i\psi\rangle_1\langle k\psi|\\ &\otimes|j\psi_\perp\rangle_2\langle(j+k-i)\psi_\perp|\\ &+\sum_{i=0}^{\infty}\sum_{j=i}^{\infty}\sum_{k=0}^{\infty}\left[\hat{\rho}_{\mathcal{A}}^{1\psi}(T_1,T_2)\right]_{ijk}^{(i\geqslant j)}|i\psi\rangle_1\langle k\psi|\\ &\otimes|j\psi_\perp\rangle_2\langle(j+k-i)\psi_\perp|,\end{aligned} \tag{A13}$$

where the coefficients for $i\geqslant j+1$ and $i\leqslant j$ are given by

$$\begin{aligned}&\left[\hat{\rho}_{\mathcal{A}}^{1\psi}(T_1,T_2)\right]_{ijk}^{(i\geqslant j)}\\ &=\frac{1}{C^4}\Gamma^{i+k-2}\frac{T_1^{(i+k)/2}T_2^{(2j+k-i)/2}R_2^{i-j-1}\sqrt{i!k!}}{(i-j-1)!\sqrt{j!(j+k-i)!}}\\ &\quad\times{}_2F_1(1+i,1+k,i-j;\Gamma^2R_1R_2),\end{aligned} \tag{A14}$$

$$\begin{aligned}&\left[\hat{\rho}_{\mathcal{A}}^{1\psi}(T_1,T_2)\right]_{ijk}^{(i<j)}\\ &=\frac{1}{C^4}\Gamma^{2j+k-i}(j+1)(j+k-i+1)\\ &\quad\times\frac{T_1^{(i+k)/2}T_2^{(2j+k-i)/2}R_1^{j-i+1}\sqrt{j!(j+k-i)!}}{(j-i+1)!\sqrt{i!k!}}\\ &\quad\times{}_2F_1(2+j,2+j+k-i,2+j-i;\Gamma^2R_1R_2).\end{aligned} \tag{A15}$$

According to previous considerations, the density matrices of states $\hat{\rho}_{\mathcal{A}'}^{0}(T_1,T_2)$ and $\hat{\rho}_{\mathcal{A}'}^{1\psi_\perp}(T_1,T_2)$ for amplifier $\mathcal{A}'$ can be directly derived from Eqs. (A8)–(A10) and (A13)–(A15) by substituting (Γ) with $(-\Gamma)$ and by relabeling the indexes describing the spatial and polarization modes. Finally, the complete output state can be reconstructed as

$$\hat{\rho}^{1\psi}(T_1,T_2) = \hat{\rho}_{\mathcal{A}}^{1\psi}(T_1,T_2)\otimes\hat{\rho}_{\mathcal{A}'}^{0}(T_1,T_2). \tag{A16}$$

2. Density matrix coefficients on the reduced $\mathbf{k}_1$ spatial mode for the amplified states

In this section we report the expression of the coefficients for the reduced density matrix on spatial mode $\mathbf{k}_1$ of $|\Phi^{1\psi}\rangle$ after propagation over a lossy channel. This result has been exploited in the calculation of the Bures distance, where the action of the orthogonality filter device has been analyzed. The starting point of the calculation is expression (A5) of $|\Phi^{1\psi}\rangle$. After the partial trace in mode $\mathbf{k}_2$, the density matrix $\hat{\rho}_{\mathbf{k}_1}^{1\psi} = \mathrm{Tr}_{\mathbf{k}_2}[|\Phi^{1\psi}\rangle\langle\Phi^{1\psi}|]$ reads

$$\begin{aligned}\hat{\rho}_{\mathbf{k}_1}^{1\psi} = &\sum_{n=0}^{\infty}\sum_{m=0}^{\infty}\frac{\Gamma^{2n+2m}}{C^6}(n+1)\\ &\times|(n+1)\psi\rangle_1\langle(n+1)\psi|\otimes|m\psi_\perp\rangle_1\langle m\psi_\perp|.\end{aligned} \tag{A17}$$

Finally, application of the lossy channel map leads to the following density matrix:

$$\hat{\rho}^{1\psi}_{\mathbf{k}_1}(T) = \sum_{i=0}^{\infty}\sum_{j=0}^{\infty}\left[\rho^{1\psi}_{\mathbf{k}_1}(T)\right]_{ij}|i\psi\rangle_1\langle i\psi| \otimes |j\psi_\perp\rangle_1\langle j\psi_\perp|, \tag{A18}$$

where the coefficients are given by

$$\left[\rho^{1\psi}_{\mathbf{k}_1}\right]_{ij} = \frac{\Gamma^{2i+2j-2}}{C^6}T^{i+j}[i+\Gamma^2 R] \times [1-\Gamma^2 R]^{-3-i-j}. \tag{A19}$$

[1] W. H. Zurek, Rev. Mod. Phys. **75**, 715 (2003).
[2] W. Schleich, M. Pernigo, and F. Le Kien, Phys. Rev. A **44**, 2172 (1991).
[3] D. M. Greenberger, M. A. Horne, and A. Zeilinger, *Bell's Theorem, Quantum Theory, and Conceptions of the Universe* (Kluwer Academic, Dordrecht, 1989).
[4] F. De Martini, Phys. Rev. Lett. **81**, 2842 (1998).
[5] F. De Martini, Phys. Lett. A **250**, 15 (1998).
[6] E. Nagali, T. De Angelis, F. Sciarrino, and F. De Martini, Phys. Rev. A **76**, 042126 (2007).
[7] F. De Martini, F. Sciarrino, and C. Vitelli, Phys. Rev. Lett. **100**, 253601 (2008).
[8] P. Sekatski *et al.*, Phys. Rev. Lett. **103**, 113601 (2009).
[9] N. Spagnolo *et al.*, e-print arXiv:1006.4325.
[10] F. De Martini, F. Sciarrino, and N. Spagnolo, Phys. Rev. A **79**, 052305 (2009).
[11] F. De Martini, F. Sciarrino, and N. Spagnolo, Phys. Rev. Lett. **103**, 100501 (2009).
[12] F. De Martini and F. Sciarrino, Prog. Quantum Electron. **29**, 165 (2005).
[13] F. De Martini, F. Sciarrino, and V. Secondi, Phys. Rev. Lett. **95**, 240401 (2005).
[14] F. De Martini and F. Sciarrino, J. Phys. A **40**, 2977 (2007).
[15] D. Bures, Trans. Am. Math. Soc. **135**, 199 (1969).
[16] M. Hubner, Phys. Lett. A **163**, 239 (1992).
[17] R. Jozsa, J. Mod. Opt. **41**, 2315 (1994).
[18] D. Pelliccia, V. Schettini, F. Sciarrino, C. Sias, and F. De Martini, Phys. Rev. A **68**, 042306 (2003).
[19] F. De Martini, D. Pelliccia, and F. Sciarrino, Phys. Rev. Lett. **92**, 067901 (2004).
[20] F. De Martini, V. Buzek, F. Sciarrino, and C. Sias, Nature (London) **419**, 815 (2002).
[21] A. Peres, *Quantum Theory: Methods and Concepts* (Kluwer Academic, Dordrecht, 1995).
[22] B. Huttner, A. Muller, J. D. Gautier, H. Zbinden, and N. Gisin, Phys. Rev. A **54**, 3783 (1996).
[23] F. Sciarrino and F. De Martini, Phys. Rev. A **72**, 062313 (2005).
[24] F. Sciarrino and F. De Martini, Phys. Rev. A **76**, 012330 (2007).
[25] J. Cai, S. Popescu, and H.-J. Briegel, e-print arXiv:0809.4906.
[26] G. S. Engel *et al.*, Nature (London) **446**, 782 (2007).
[27] G. A. Durkin, C. Simon, J. Eisert, and D. Bouwmeester, Phys. Rev. A **70**, 062305 (2004).
[28] L. J. Slater, *Generalyzed Hypergeometric Functions* (Cambridge University Press, Cambridge, 1966).